

01 Jan 2003

## A Single-Element Tuning Fork Piezoelectric Linear Actuator

J. Satonobu

K. Nakamura

S. Ueha

Daniel S. Stutts

*Missouri University of Science and Technology*, stutts@mst.edu

*et. al.* For a complete list of authors, see [https://scholarsmine.mst.edu/mec\\_aereng\\_facwork/3398](https://scholarsmine.mst.edu/mec_aereng_facwork/3398)

Follow this and additional works at: [https://scholarsmine.mst.edu/mec\\_aereng\\_facwork](https://scholarsmine.mst.edu/mec_aereng_facwork)

 Part of the [Aerospace Engineering Commons](#), and the [Mechanical Engineering Commons](#)

---

### Recommended Citation

J. Satonobu et al., "A Single-Element Tuning Fork Piezoelectric Linear Actuator," *IEEE Transactions on Ultrasonics, Ferroelectrics and Frequency Control*, Institute of Electrical and Electronics Engineers (IEEE), Jan 2003.

The definitive version is available at <https://doi.org/10.1109/TUFFC.2003.1182121>

This Article - Journal is brought to you for free and open access by Scholars' Mine. It has been accepted for inclusion in Mechanical and Aerospace Engineering Faculty Research & Creative Works by an authorized administrator of Scholars' Mine. This work is protected by U. S. Copyright Law. Unauthorized use including reproduction for redistribution requires the permission of the copyright holder. For more information, please contact [scholarsmine@mst.edu](mailto:scholarsmine@mst.edu).

# A Single-Element Tuning Fork Piezoelectric Linear Actuator

James R. Friend, *Member, IEEE*, Jun Satonobu, Kentaro Nakamura, Sadayuki Ueha, and Daniel S. Stutts

**Abstract**—This paper describes the design of a piezoelectric tuning-fork, dual-mode motor. The motor uses a single multilayer piezoelectric element in combination with tuning fork and shearing motion to form an actuator using a single drive signal. Finite-element analysis was used in the design of the motor, and the process is described along with the selection of the device's materials and its performance. Swaging was used to mount the multilayer piezoelectric element within the stator. Prototypes of the 25-mm long bidirectional actuator achieved a maximum linear no-load speed of 16.5 cm/s, a maximum linear force of 1.86 N, and maximum efficiency of 18.9%.

## I. INTRODUCTION

PIEZOELECTRIC motor systems exploit the transduction phenomenon from electrical energy input to mechanical energy output within piezoelectric materials. The solid-state construction possible with such devices, coupled with their peculiar advantages over standard electromagnetic motors, is constrained by their sensitivity to heat, relatively low efficiency, and short operating life [1]. However, inroads are being made on these problems, and commercially useful actuators are becoming more common. This paper, a small step in this process, details the design, construction, and testing of a small single-piezoelectric element linear actuator for low-voltage applications.

Some piezoelectric motor systems have been commercially successful due to their extraordinarily high torque; Toshiiku Sashida's Shinsei (Shinsei Corporation, Tokyo, Japan) motor [2], [3] is an excellent example. Others have been successful because they are extremely tiny; Seiko's (Seiko Epson Corporation, Tokyo, Japan) 8 mm motor [4], [5] is used in watches to turn an eccentric disk to act as a silent alarm. More recent linear motor designs are extremely powerful and demonstrate the extraordinary sliding forces possible using large piezoelectric actuators [6], [7]. Still others are successful because the motion they develop is linear, extremely precise, or both.

Uchino and Ohnishi [8] and their associates at ALPS Corporation, Niigata, Japan, developed small linear motors using either one or two multilayer piezoelectric actuators (MLPA). In one version [8], an MLPA was placed horizontally in between the top arms of an H-structure. The bottom arms of the H-structure acted against a slider, and each arm possessed a different resonance frequency. The direction of the slider was controlled by changing the frequency of excitation from the resonance frequency of the left leg to the resonance frequency of the right leg. In a similar vein, an inverted U-shaped structure was used with the MLPA placed between the legs. But the MLPA remained parallel with the sliding surface, and the different resonance frequencies of the legs were exploited to obtain sliding motion. With these designs, one of the two legs was pulled, essentially statically, behind the structure as it moved against the slider, and the placement of the MLPA parallel to the sliding surface prevented generation of significant motion perpendicular to the sliding surface.

In another version [9], [10], either one or two MLPAs were used to excite elliptical motion along the output end of a simple I-shaped beam, with the MLPAs placed at an angle at the top of the beam. The output, at the bottom of the beam, was used by placing the beam perpendicular to the slider. For the single-MLPA version, the direction of motion was changed by changing the excitation frequency over several tens of kilohertz. For the double-MLPA version, the direction of motion was reversed by reversing the  $\lambda/4$  temporal phase difference of excitation between the two MLPAs. Another double-MLPA version used a so-called  $\Pi$ -shaped structure, with two MLPAs placed at an angle at the top corners of the structure. The slider was placed against the bottom legs of the structure. In each of these designs, one end of the MLPA remains unattached; the deformation of the MLPA at that end during vibration is not used in the operation of the actuators and, therefore, does not make full use of the MLPAs deformation.

The device described herein is a small tuning-fork-shaped linear actuator designed to address some of the shortcomings of the Alps motors, using, to the knowledge of the authors, previously unpublished construction techniques. Inherent in its design is the use of a single MLPA enclosed in the structure, placed at an angle with respect to the sliding surface. As a result, both ends of the MLPA are used to excite motion not only along the sliding surface, but also perpendicular to it, enhancing the contact forces between the actuator and slider. Furthermore, the design of the actuator is tailored to match the resonance frequencies of the forks, enabling both forks to participate in the

Manuscript received June 12, 2002; accepted September 10, 2002. The authors appreciate support of this work by grants 0-5-2G010867, 0-5-2G113786 from Honeywell, NSF grant CMS-9409937, and a grant-in-aid from the Japanese Ministry of Education, Culture, Sports, Science and Technology.

R. Friend, K. Nakamura, and S. Ueha are with the Precision and Intelligence Laboratory, Tokyo Institute of Technology, Yokohama, Japan (jamesfriend@ieee.org).

J. Satonobu is with the Department of Mechanical Engineering, University of Hiroshima, Hiroshima, Japan.

D. S. Stutts is with the Department of Mechanical and Aerospace Engineering and Engineering Mechanics at the University of Missouri-Rolla, Rolla, MO.

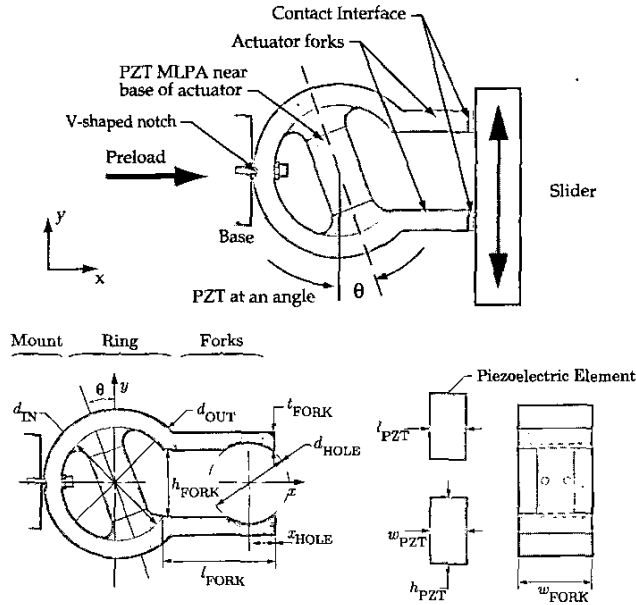


Fig. 1. The tuning fork actuator concept.

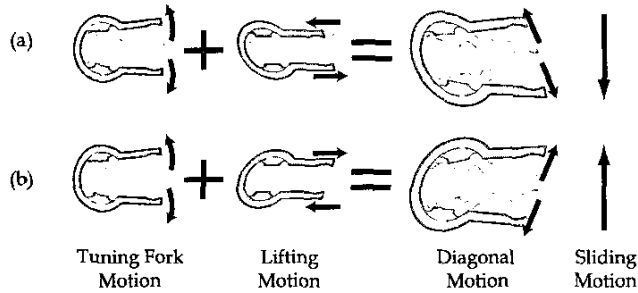


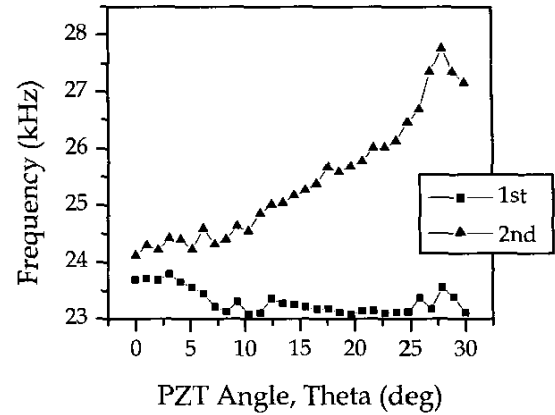
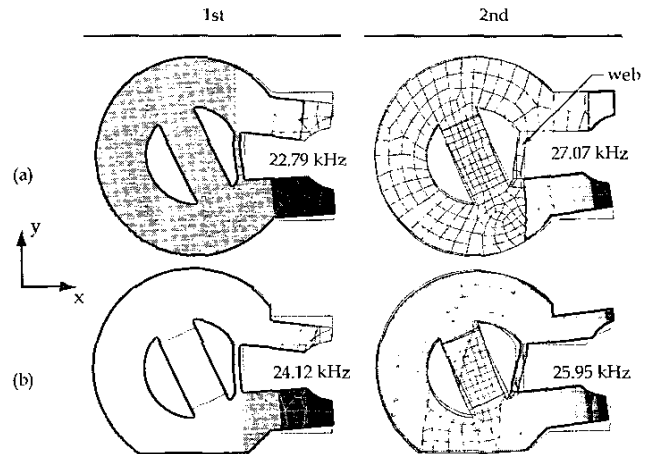
Fig. 2. Generating diagonal motion along the stator forks.

operation of the actuator in both directions. By mounting the MLPA in the actuator, it may be compressively prestressed, enhancing the MLPA's longevity [11].

When operated at its design frequencies, the actuator uses a relatively low voltage, roughly  $5 V_{RMS}$ . This feature serves as an advantage in high-altitude, spacecraft, or Martian atmospheres in which ionization of the gas surrounding the actuator could permit arcing even at modest voltages [12], and that advantage is one of the reasons for pursuing this study.

## II. DESIGN

The tuning fork device retains the traditional arrangement of a piezoelectric actuator: piezoelectric material exciting ultrasonic vibration in a metal stator to move a surface in contact, the slider, (Fig. 1). By placing the piezoelectric material at an angle,  $\theta$ , simple tuning-fork motions married with fork-lifting motions, as shown in Fig. 2, can generate diagonal motion along the contact interface. This motion then can be used to move the slider. When the stack angle,  $\theta$ , is zero, the mode shapes of the stator

Fig. 3. The resonance frequencies of the two fundamental tuning-fork/lifting modes versus MLPA angle,  $\theta$ , denoted 1st and 2nd.Fig. 4. Compensating for the asymmetry in the stator. Finite element analysis results of the first two tuning/lifting fork modes (a) with no compensation, (b) with grinding of the top fork (1.5 mm) and bottom of the ring section (2 mm). Note the addition of the web in the structure and the asymmetric motion of the forks in the original configuration. The shading indicates displacement in the  $y$ -direction.

that can be driven by the PZT are all tuning fork motions. However, once the PZT is turned, each of these modes separate into two different modes because of the introduction of asymmetry in the stator. Because the PZT is turned, the top fork is longer, causing its resonance to occur at a lower frequency than the bottom fork. For example, the fundamental tuning-fork mode in this case separates into a motion dominated by the top fork, followed by motion appearing mostly in the lower fork, at a higher frequency. The separation in frequency of the two modes that arise from the fundamental tuning-fork mode is shown in Fig. 3. For  $\theta = 25^\circ$ , the asymmetric motion is illustrated in Fig. 4(a). Coincidentally, a 1-mm thick web was placed across the forks to increase the resonance frequencies of all the modes above the audible range; the data reported was calculated from a stator with the web. In these figures, the two modes are referred to as the first and second fundamental tuning

fork/lifting modes. Note the first mode has motion mostly in the top leg, and the second mode's motion is within the bottom leg, with a frequency separation between them of about 5 kHz. The frequency separation needs to be reduced to cause a more balanced response among the two legs.

Early in the design process, the values of the parameters used to define the stator's geometry were changed in an attempt to bring these two mode shapes' resonance frequencies closer together, as shown in Fig. 5. But this was not possible because the asymmetry of the stator remained. However, by grinding away part of the bottom of the ring and the top side of the top fork, the asymmetry was compensated. The grinding along the bottom ring lowered its stiffness and, therefore, its resonance frequency; grinding the top fork near its end lowered its mass and, therefore, raised its resonance frequency.

By making these changes, the forks' displacement magnitude moved much closer together. The ratio of maximum displacement of the tip of the top fork to the tip of the bottom fork in the  $y$ -direction was originally 2.02 at 22.7 kHz and 5.8 at 27.1 kHz in Fig. 4(a), but became 1.58 at 24.1 kHz and 1 at 25.9 kHz, respectively.

Also important, however, is generating bidirectional motion. Though there are several ways to achieve this, the simplest method is first to align the modes as much as possible, then use a second or higher harmonic of the paired fundamental tuning-fork/lifting modes. This way, the phase between the tuning-fork motion and the lifting motion explicitly depends on the mode shape throughout the resonance peak. In Fig. 4 the phasing of the legs at 24.12 kHz is not useful for motion—the legs move together and apart at the same time. At 25.95 kHz, the motion is better, with the forks moving in the same direction and with a strong lifting motion, generating diagonal motion with a ratio of maximum  $x$ -to- $y$  displacement of 0.72 for the top fork and 0.55 for the bottom fork, as calculated in ANSYS. Several modes between 20 and 75 kHz are illustrated in Fig. 6. Some of these modes have synchronized tuning-fork motion and large fork-lifting motions, and thus may be useful for generating sliding. The mode shape at 25.95 kHz, discussed before, is such a mode, as are the modes at 52.01 and 58.58 kHz. Others, including the mode at 44.07 kHz, have out-of-plane motion or have motion someplace other than the fork tips. The mode at 74.72 kHz has significant fork motion, but it also has large displacements within the ring part of the stator.

The direction of motion is controlled by the orientation of the diagonal motion generated at the fork tips, as shown in Fig. 2. If the diagonal motion is oriented upward as the forks approach the slider, they will move the slider upward. The difference in the normal force, and therefore the sliding force, as the forks move toward and away from the slider make this motion possible. To change the direction of sliding motion, the orientation of the diagonal fork motion must be changed. One way to achieve this is to use other modes that have the other fork motion orientation. In other words, the direction of sliding is reversed by

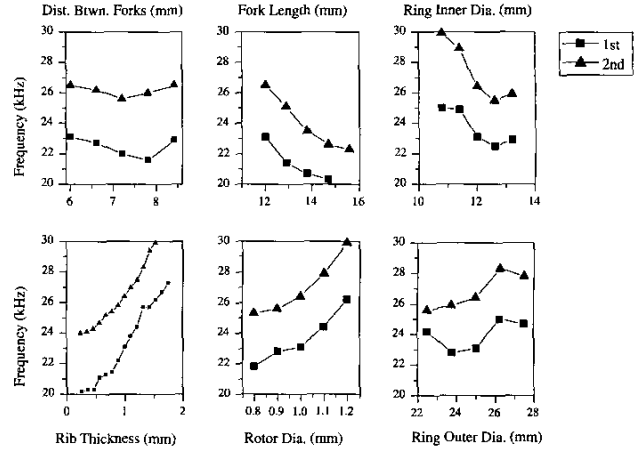
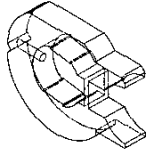


Fig. 5. Resonance frequencies of the two fundamental tuning-fork modes versus six geometry parameters; 1st and 2nd indicate the lower and higher frequency fundamental tuning-fork/lifting modes, respectively.

TABLE I  
FINAL DIMENSIONS OF THE TUNING FORK ACTUATOR.

Parameter	Value (mm)*	Geometry
$d_{IN}$	12	
$d_{OUT}$	25	
$\theta$	25	
$h_{FORK}$	6	
$t_{FORK}$	5	
$l_{FORK}$	12	
$w_{FORK}$	5	
$d_{HOLE}$	10	
$x_{HOLE}$	0	
$l_{PZT}$	5	
$w_{PZT}$	5	
$h_{PZT}$	10	

\*Refer to Fig. 1 for parameter definitions.

changing the frequency of excitation, thus the difference between the motions in Fig. 2(a) and (b). The dimensions of the final design for the stator is given in Table I.

### III. ACTUATOR AND TEST FIXTURE CONSTRUCTION

The stator was machined using computer numerically controlled milling of C1020 low-corrosion steel plate. The fork tips and MLPA mounts were polished to a  $5\text{-}\mu\text{m}$  finish in preparation for mounting friction material and the MLPA. The MLPA was placed within the stator and checked for a snug fit, taken out and replaced with epoxy along the interfaces between the MLPA and stator, and mechanically secured in place by swaging the stator at two or more places near the mounting interfaces, as shown in Fig. 7.

The swaging was performed before the epoxy cured. In early trials, the epoxy was allowed to cure before swaging, but the coupling of the stator to the piezoelectric material

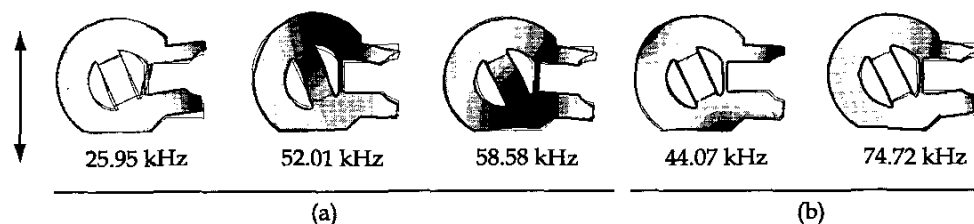


Fig. 6. Predicted mode shapes according to finite element analysis. The contours indicate the relative magnitude of deflection in the direction of the arrow shown on the left (except for the plot at 44.07 kHz, which indicates deflection in and out of the page) for (a) modes that might be useful for actuation, and (b) modes that are to be avoided.

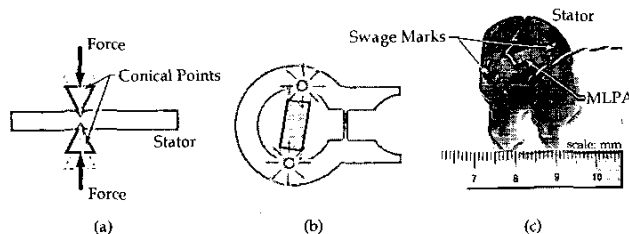


Fig. 7. Mounting the MLPA within the stator using swaging (a) causes (b) expansion of the stator material near the MLPA, securing it, as shown in a prototype (c).

was poor. The depth of the swage and number of swage operations also affects the coupling of the MLPA and stator; having too many or pressing too deeply causes unwanted flexibility near the MLPA. Swaging accomplishes three goals: firmly coupling the piezoelectric material to the stator on both ends; placing the MLPA under compressive prestress, thus enhancing its durability [11]; and thinning the epoxy bond. Though it is probably possible to eliminate the use of epoxy to bond the MLPA to the stator, it was not tried for these prototypes.

Two materials were used for contact on the stator, alumina and asbestos brake liner material. For the slider, alumina was used throughout. In particular, the alumina/alumina interface has been shown to be a durable and convenient choice [13], [14]. In each case, the materials were polished to 0.5 ~ 1 mm thickness and bonded to the stator using the same Loctite epoxy. The thickness of the epoxy was minimized by fastening the parts in a precision milling vise during curing.

The contact counterfaces were polished to 3  $\mu\text{m}$  roughness, using either increasingly fine sandpaper or several grades of diamond grit lapping powder in oil on a tool steel polishing plate. In either case, final hand polishing was performed using standard writing paper and alcohol on a flat glass plate.

A small, v-shaped notch was machined into the ring section of the stator (see Fig. 1), along with a 3-mm threaded hole to receive a bolt to provide a secure mount. This mount prevented turning of the stator to ensure the feet of the stator were in parallel contact with the slider.

A test fixture was constructed to hold the stator and slider, and to permit measurement of the actuator's performance. The test fixture's arrangement is shown in Fig. 8. A

piece of alumina plate, polished to have parallel faces, was mounted onto a light sliding platform with a small linear bearing to form the slider. An encoder grating, made by printing a regular pattern of lines on an overhead transparency on a laser printer, was attached to the slider's end. By mounting an inexpensive optoelectronic switch, with the encoder serving as the gate in conjunction with a digital oscilloscope and some software, it was relatively easy to measure the velocity of the slider with respect to time. A drawback of this approach is the low resolution of the velocity signal, particularly during the start of the sliding motion when the actuator is capable of accelerating the slider over a very short distance. However, for this study, the measurement of the acceleration with large masses placed on the monofilament line was still possible. The preload force was placed upon the actuator by using a preload spring to press against the actuator's mounting, which was free to slide vertically; the preload was determined by measuring the deflection distance in this spring.

#### IV. RESULTS

The actuator's electrical, vibration, and linear actuation characteristics were measured; the results are indicated in the following sections.

##### A. Electrical Characteristics

The impedance characteristics of the actuator were measured using a standard HP 4194A (Hewlett-Packard, Palo Alto, CA) analyzer at 0.5  $V_{RMS}$ . From Fig. 9(a), the two modes at 24–25 kHz appear, with the cross ("x") and the double circle ("⊙") indicating not useful and very useful modes, respectively. The modes appearing at 47 and 57 kHz correspond to the 52 and 58 kHz modes in the ANSYS analysis, and are both marked as being useful; the shift is due to the assumption of an ideally fixed base (see Fig. 1). The actual base can vibrate along with the actuator, and these modes have motion at the base, unlike the mode at 26 kHz; the consequence is the modes' frequencies are reduced. Not surprisingly, the undesirable mode that appears in ANSYS at 44 kHz does not appear in the impedance test; it cannot be driven by the MLPA. Though not very prominent, there is a slight peak at 59 kHz that indicates another out-of-plane mode. At 74 kHz, the mode corresponds to the ANSYS analysis. Although not very

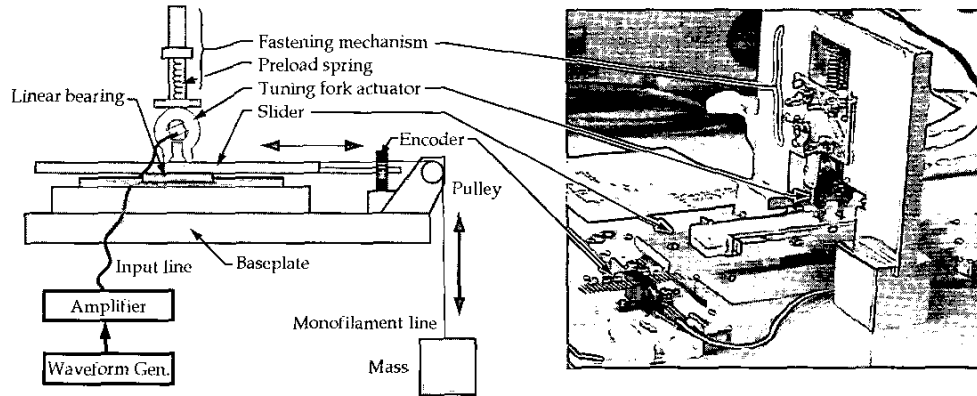


Fig. 8. The test fixture.

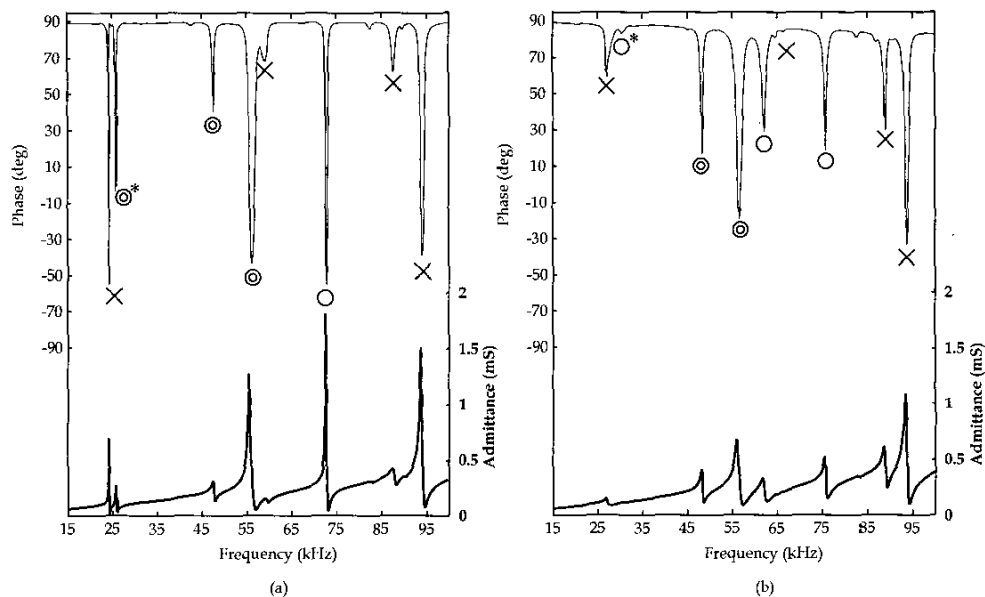


Fig. 9. Impedance amplitude and phase characteristics of the stator with respect to excitation frequency (a) without slider and (b) with a slider at 1.98 N preload; "x" indicates a useless mode, "O" a potentially useful mode, and "⊙" a useful mode.

useful, it is marked with a single circle ("O"), implying it potentially could be useful because it does possess fork motion. Above this mode, however, the motions are primarily within the MLPA, and so are of little use for actuation.

Placing the stator into contact with a slider caused significant change in the impedance spectrum, as shown in Fig. 9(b). The contact interface was alumina/alumina, though other contact interfaces produced similar results. In particular, the mode at 47 kHz amplified enough to become useful, as will be shown later. Unfortunately, the reverse is also true; the useful mode at 25.25 kHz, indicated with an asterisk in Fig. 9, almost disappeared when the slider was introduced. Certainly the introduction of the slider also alters the mode shapes, just as it has altered the impedance spectrum, but the effect was not included in the finite element analysis due to the extraordinary expense of contact analysis.

Fig. 10 illustrates the effect of swaging the stator on the impedance. Before the swaging was performed, an MLPA was mounted in a stator using epoxy with a press fit tolerance. After the epoxy cured, the impedance spectrum for the unswaged stator was measured. Subsequently, the stator was swaged, and the impedance spectrum for the swaged version was measured. Notice that the general effect is the larger minimum phase for most resonances, indicating an improved coupling between the stator and MLPA and, perhaps, indicating improvement from the static compression of the MLPA within the stator. Furthermore, the resonances are generally narrower, especially the large peak at around 55 kHz, representing an increase in the quality factor from 35 to 110 for this particular peak. Another effect of the swaging is the lowering of the resonance frequencies of many of the modes, from 1 to as much as 5 kHz. The reason for this shift is the increased flexibil-

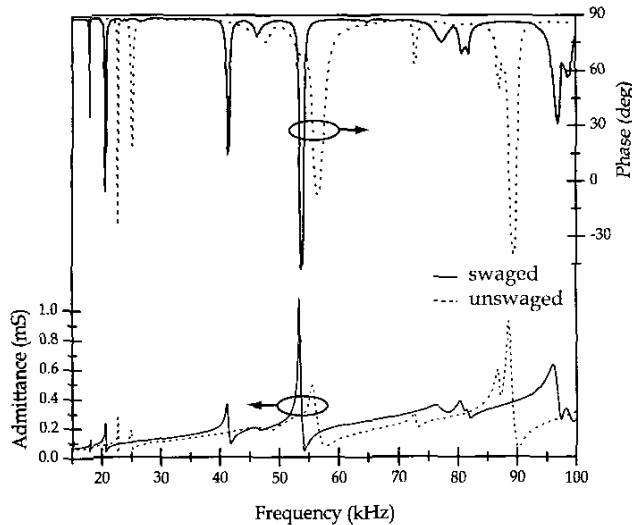


Fig. 10. Admittance and phase with respect to excitation frequency, with MLPA, swaged and unswaged. The arrows indicate the relevant axis for each curve.

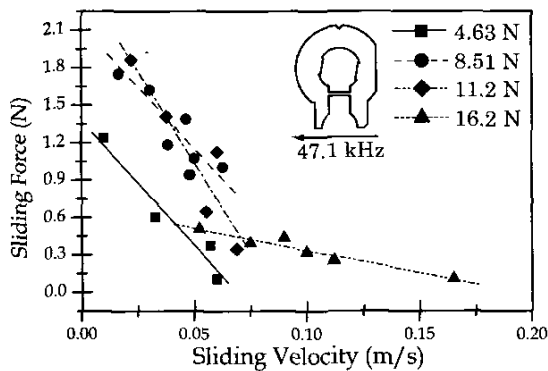


Fig. 11. Sliding force versus sliding velocity with brake liner/alumina contact counterfaces at 47.1 kHz. The lines represent least-square fits of the data.

ity in the stator around the swaged area, which obviously affects the mode shape. However, the benefit of increased response was believed to outweigh this problem, and so all stators used in testing reported here were swaged.

### B. Linear Motion Results

Using the test fixture in Fig. 8, measurements of the slider's velocity with respect to sliding force, preload, voltage applied to the MLPA, stator version, and mass on the monofilament line were made. From these measurements, the axial force the stator could deliver to the slider based on these variables was determined.

Figs. 11 and 12 plot the sliding force and efficiency versus sliding velocity at a frequency of 47.1 kHz, using brake liner/alumina contact counterfaces. Figs. 13 and 14 provide the same data but at 55.3 kHz, at which the actuator moved in the opposite direction. The efficiency is defined here as the power out, or sliding force times the

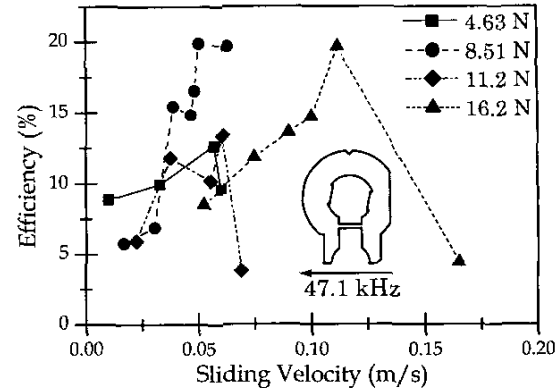


Fig. 12. Efficiency versus sliding velocity with brake liner/alumina contact counterfaces at 47.1 kHz.

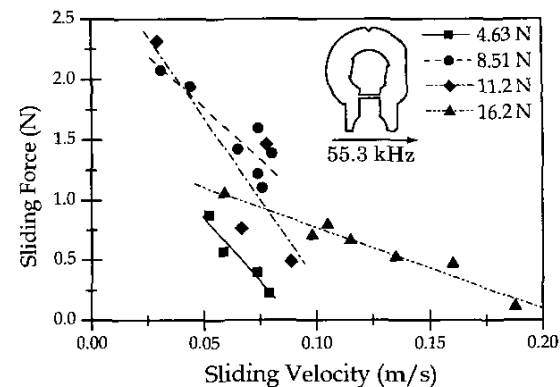


Fig. 13. Sliding force versus sliding velocity with brake liner/alumina contact counterfaces at 55.3 kHz. The lines represent least-square fits of the data.

sliding velocity, divided by true average power in, or the time-average of the product of the instantaneous voltage times the instantaneous current (taking the phase into account). The 47.1 and 55.3 kHz resonances correspond to the 52 kHz and 58 kHz mode shapes in Fig. 5, respectively, with the shift being due to the flexibility of the base and the swaging of the stator. The applied voltage in all cases was 3.5  $V_{RMS}$ , with a positive direct current (DC) bias of 2.5 V to maintain the poling within the MLPA.

Maximum sliding forces of 1.86 and 2.31 N were reached using a preload of 11.27 N in the 47.1 and 55.3 kHz directions, while maximum velocities of 16.5 and 18.8 cm/s, were reached at a preload of 16.2 N in the 47.1 and 55.3 kHz directions, respectively. A maximum efficiency of 19.7% was reached in the 47.1 kHz direction at a sliding velocity of 11.2 cm/s using a preload of 16.2 N. In the 55.3 kHz direction, the efficiency peaked at 18.9% at the same preload and a sliding velocity of 11.5 cm/s.

From 4.63 N to 11.2 N of preload, the trend of the actuator's response is generally toward larger sliding force/velocity, but the higher 16.2 N preload gives a different response, with a dramatically higher sliding velocity and reduced sliding force. This possibly could be to a

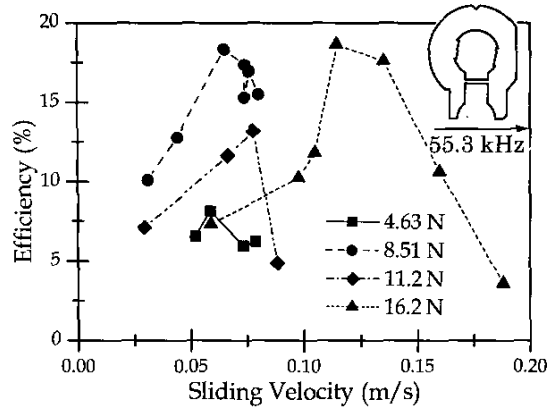


Fig. 14. Efficiency versus sliding velocity with brake liner/alumina contact counterfaces at 55.3 kHz.

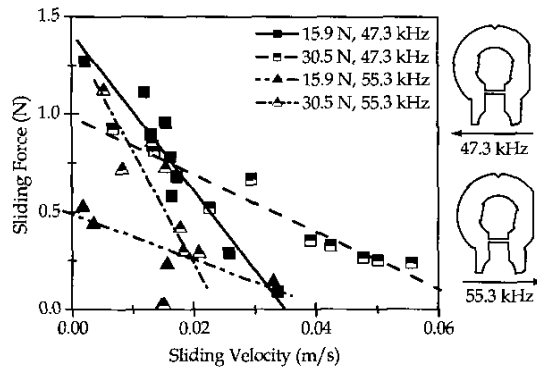


Fig. 15. Sliding force versus velocity for alumina/alumina contact counterfaces at 47.3 kHz and 53.3 kHz. The lines represent least-square fits of the data.

change in the motion along the contact interface from redistribution of the contact force along the interface. The brake liner material's compliance, at low preload serves to transmit the vibration of the stator to the slider without much effect on the stator's vibration. At a higher preload, beyond 10 N or so, the friction liner material may be fully compressed.

For an alumina/alumina contact interface, Figs. 15 and 16 indicate the force versus velocity and efficiency versus velocity in both sliding directions, respectively. Because the counterfaces are far stiffer, a higher preload is necessary, which requires a higher applied voltage of  $4.20 V_{RMS}$  to excite sufficient vibration in the structure. A positive DC bias of 2 V also was applied. The direction of sliding is indicated in Fig. 15.

At a preload of 15.9 N, the maximum measured sliding forces were 1.27 and 0.524 N; the maximum velocities were 3.38 cm/s and 3.57 cm/s in the 47.3 and 55.3 kHz directions, respectively. At 30.5 N preload, the sliding forces and velocities peaked at 0.927 and 1.12 N, and 5.56 and 2.08 cm/s in the 47.3 and 55.3 kHz directions. The efficiency of this configuration is consistently lower than the alumina/brake liner configuration, with a maximum of

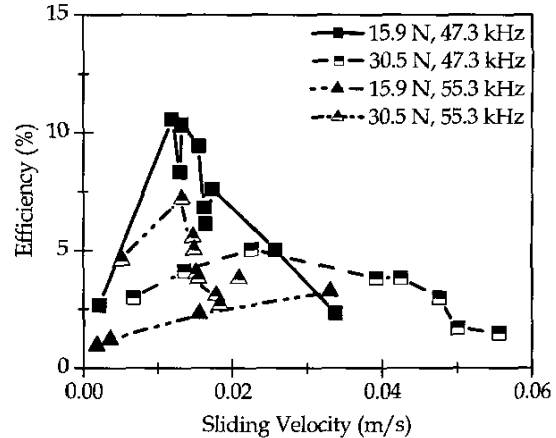


Fig. 16. Efficiency versus velocity for alumina/alumina contact counterfaces at 47.3 kHz and 53.3 kHz.

10.3% at 1.32 cm/s, 15.9 N preload, and in the 47.3 kHz direction. Generally, the efficiency is less than 5%.

## V. CONCLUSIONS

A novel piezoelectric linear actuator was presented, using a single piezoelectric element mounted in the stator structure with swaging. The basic concept, along with its improvement via finite element analysis, was shown. For a few select choices of two different stator designs and three different contact materials, the impedance characteristics of the stator along with the performance of the actuator were measured. The experimental results demonstrate the feasibility of the design concept.

Bidirectional motion, with a maximum sliding force of 1.86 N and a maximum velocity of 16.5 cm/s in either direction, was obtained using alumina/brake liner contact. The efficiency of the alumina/brake liner actuator was about 10%, but it achieved a maximum efficiency of 18.9%.

Using an alumina/alumina interface, bidirectional motion was obtained; but the efficiency was much lower, generally less than 5%. From the alumina/alumina actuator, a maximum (bidirectional) sliding force of 0.927 N and velocity of 3.38 cm/s were obtained. Though alumina/alumina interfaces have been successful in some piezoelectric actuator designs, in this case the more compliant alumina/brake liner contact interface performs far better, particularly with regard to the maximum sliding velocity.

For future work, the authors would like to pursue the revision of this actuator to improve upon the design of the stator, using hard PZT multilayer piezoelectric actuators in order to improve the efficiency of the system at ultrasonic frequencies. Furthermore, the authors envision a detailed study of the fork arms' motion and their shape to obtain improved performance. Using this actuator for sliding perpendicular to the forks, or rotation of a shaft placed between the forks, will be considered.



## ACKNOWLEDGMENT

The authors would like to acknowledge the assistance of Dr. Takaaki Ishii, without whom this work would have been impossible.

## REFERENCES

- [1] S. Ueha and Y. Tomikawa, *Ultrasonic Motors—Theory and Applications*, ser. Monographs in Electrical and Electronic Engineering, vol. 29, Oxford: Clarendon Press, 1993.
- [2] T. Sashida, "Supersonic vibration driven motor device," U.S. Patent 4,548,090, Oct. 22, 1985.
- [3] T. Sashida, "Motor device utilizing ultrasonic oscillation," U.S. Patent Number 4,562,374, Dec. 31, 1985.
- [4] M. Kasuga, T. Mori, and N. Tsukada, "Travelling-wave motor," U.S. Patent Number 5,006,746, Apr. 9, 1991.
- [5] M. Kawata, F. Ozawa, M. Kasuga, M. Suzuki, and T. Shibayama, "Ultrasonic motor," U.S. Patent Number 5,091,670, Feb. 25, 1992.
- [6] C.-H. Yun, T. Ishii, K. Nakamura, S. Ueha, and K. Akashi, "A high power ultrasonic linear motor using a longitudinal and bending hybrid bolt-clamped langevin type transducer," *Jpn. J. Appl. Phys.*, vol. 40, no. 5B, pp. 3773–3776, 2001.
- [7] M. K. Kurosawa, O. Kodaira, Y. Tsuchitoi, and T. Higuchi, "Transducer for high speed and large thrust ultrasonic linear motor using two sandwich-type vibrators," *IEEE Trans. Ultrason., Ferroelect., Freq. Contr.*, vol. 45, no. 5, pp. 1188–1195, 1998.
- [8] K. Uchino and K. Ohnishi, "Linear motor," U.S. Patent Number 4,857,791, Aug. 15, 1989.
- [9] K. Ohnishi and K. Yamakoshi, "Ultrasonic linear actuator using coupled vibration," *J. Acoust. Soc. Amer.*, vol. 11, no. 4, pp. 235–241, 1990.
- [10] K. Ohnishi, K. Naito, and T. Nakazawa, "Ultrasonic wave linear motor," U.S. Patent Number 5,216,313, June 1, 1993.
- [11] "Multilayer piezoelectric actuators (chounpa denki akuchuyata)," Report EC-011, Vol. 3, Tokin Co., Ltd., 1997. (in Japanese)
- [12] T. Swindle, A. Chutjian, J. Hoffman, J. Jordan, J. Kargel, R. McEntire, and L. Nyquist, "Isotopic analysis and evolved gases," in *Planetary Surface Instruments Workshop*, T. Kostiuk, C. Meyer, and A. Treiman, Eds. 1996, pp. 21–40.
- [13] T. Ishii and K. Uchino, "Ultrasonic motor using alumina ceramics," in *89th Annu. Meeting*, American Ceramic Society, 1987, pp. 124–128.
- [14] P. Rehbein and J. Wallaschek, "Friction and wear behaviour of polymer/steel and alumina/alumina under high-frequency fretting conditions," *Wear*, vol. 216, pp. 97–105, 1998.



**James R. Friend** (S'98–A'98–M'03) was born in Lubbock, Texas, on September 13, 1970. He received the B.S. degree in aerospace engineering, magna cum laude, and the M.S. and Ph.D. degrees in mechanical engineering from the University of Missouri-Rolla in 1992, 1994, and 1998, respectively. He received the American Society of Mechanical Engineers (ASME) Best Paper award and American Institute of Aeronautics and Astronautics (AIAA) Jefferson Goblet Student Paper Award for a paper delivered at the 97th

Annual AIAA/ASME/American Helicopter Society/American Society of Civil Engineering Structural Dynamics and Mechanics Conference in 1996. In 1999, he joined the faculty at the newly formed Department of Mechanical Engineering at the University of Colorado–Colorado Springs. He is now at the Precision and Intelligence Laboratory, Tokyo Institute of Technology, Tokyo, Japan, as a research associate, with research interests in millimeter- and micrometer-scale piezoelectric actuators and their applications.

He is a member of IEEE, ASME, and the Acoustical Society of Japan, and an associate member of Sigma Xi.

**Jun Satonobu** was born in Hiroshima prefecture, Japan, on August 1, 1964. He received the B.Eng., the M.Eng., and the D.Eng. degrees from the Tokyo Institute of Technology, Tokyo, Japan in 1987, 1989, and 1998, respectively. He has been in the Faculty of Engineering, Hiroshima University since April, 1998, and has researched as a Visiting Fellow in the Department of Mechanical and Aerospace Engineering at the University of Colorado at Colorado Springs from June, 2000 to March, 2001.

Dr. Satonobu is a member of the Acoustical Society of Japan and the Japan Society of Mechanical Engineers.



**Kentaro Nakamura** was born in Tokyo, Japan, on July 3, 1963. He received the B.Eng., the M.Eng., and the D.Eng. degrees from the Tokyo Institute of Technology, Tokyo, Japan, in 1987, 1989, and 1992, respectively. He has been an associate professor of the Precision and Intelligence Laboratory, Tokyo Institute of Technology, Tokyo, Japan, since 1996. His field of research is the application of ultrasonics and the measurement of vibration and sound using optical methods.

He has received the Awaya Kiyoshi Award for encouragement of research from the Acoustical Society of Japan in 1996. Dr. Nakamura is a member of the Acoustical Society of Japan, the Japan Society of Applied Physics, the Institute of Electrical Engineers of Japan, and the Institute of Electronics, Information and Communication Engineers.



**Sadayuki Ueha** was born in Kyoto Prefecture, Japan, on February 28, 1943. He received the B.Eng. degree in electronic engineering from the Nagoya Institute of Technology in 1965, the M.Eng. degree in 1967, and the D.Eng. degree in 1970, both in electric engineering, from the Tokyo Institute of Technology, Tokyo, Japan. He currently conducts research in high power ultrasonics. He has been a professor of the Precision and Intelligence Laboratory, Tokyo Institute of Technology, since 1992.

He is a steering committee member of the World Congress on Ultrasonics and serves as the secretariat of WCU97. He received the Best Paper Award from The Japan Society of Applied Physics in 1975 and from the Acoustical Society of Japan in 1980, respectively. Dr. Ueha is a member of the Japan Society of Applied Physics, the Acoustical Society of Japan, the Institute of Electronics, Information and Communication Engineers, and the Japan Society of Ultrasonics in Medicine. Currently he is a member of the editorial board of the journal *Ultrasonics*.



**Daniel S. Stutts** was born in Canton, GA, on January 9, 1959. He received bachelors and masters degrees in mechanical engineering from the Louisiana State University in Baton Rouge, LA in 1983 and 1987, respectively. He earned his Ph.D. in mechanical engineering in 1990 from Purdue University in West Lafayette, IN. In 1991, he joined the faculty of mechanical engineering and engineering mechanics at the University of Missouri-Rolla, Rolla, MO, and was promoted to associate professor in 1997. He has worked in the area of piezoelectric actuator design and modeling since 1993. His hobbies include cycling and music.